JACS
JOURNAL OF THE AMERICAN CHEMICAL SOCIETY

ARTICLE

pubs.acs.org/JACS

Structural and Electric Field Effects of Ions in Aqueous Nanodrops

James S. Prell, Jeremy T. O'Brien, and Evan R. Williams*

Department of Chemistry, University of California, Berkeley, California 94720-1460, United States

ABSTRACT: Ensemble infrared photodissociation (IRPD) spectra in the hydrogen stretch region (~2950−3800 cm^{-1}) are reported for $M(H_2O)_{35-37}$, with M = I^-, Cl^-, HCO_3^-, OH^-, tetrabutyl-, tetrapropyl-, and tetramethylammonium, Cs^+, Na^+, Li^+, H^+, Ba^{2+}, Ca^{2+}, Co^{2+}, Mg^{2+}, La^{3+}, and Tm^{3+}, at 133 K. A single, broad feature is observed in the bonded-OH region of the spectra that indicates that the water network in these clusters is bulk-like and likely resembles liquid water more strongly than ice. The free-OH region for all of these clusters is dominated by peaks corresponding to water molecules that accept two and donate one hydrogen bond (AAD water molecules), indicating that AAD water molecules are more abundant at the surface of these ions than AD water molecules. A-only water molecules are present in significant abundance only for the trivalent metal cations. The frequency of the AAD free-OH stretch band shifts nearly linearly with the charge state of the ion, consistent with a Stark shift attributable to the ion's electric field. From these data, a frequency range of 3704.9−3709.7 cm^{-1} is extrapolated for the free-OH of AAD water molecules at the (uncharged) bulk liquid water surface, consistent with sum-frequency generation spectroscopy experiments. Differences in both the bonded- and the free-OH regions of the spectra for these ions are attributable to ion-induced patterning of the water network that extends to the surface of the clusters, which includes water molecules in the third and fourth solvation shells; that is, these ions pattern water molecules at long distance to various extents. These spectra are simulated using two different electrostatic models previously used to calculate OH-stretch spectra of bulk water and aqueous solutions and parametrized for bonded-OH frequencies. These models qualitatively reproduce a number of features in the experimental spectra, although it is evident that more sophisticated treatment of water molecule and ion polarizability and vibrational coupling is necessary for more quantitative comparisons.

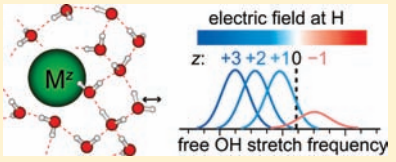

INTRODUCTION

Over 120 years ago, Franz Hofmeister observed that many ions can be ordered by their tendency to precipitate various proteins in aqueous salt solutions.[1] This "Hofmeister series" of ions has been shown to be remarkably reproducible for a variety of chemical properties, from aqueous salt solubilities[2] to cloud points of nonionic surfactants[3] and transport through ion channels,[4] yet the physical origin of the Hofmeister series is still debated.[2,5−14] In recent years, many studies have challenged traditional explanations of the Hofmeister series as originating from long-range effects of ions on the hydrogen-bonding network of bulk water, suggesting instead that this effect originates predominantly from direct ion−cosolute interactions.[2,8,12] Results from static vibrational spectroscopy,[11,13] femtosecond infrared spectroscopy (including spectral diffusion[13] and measurements of water molecule reorientation times[15−17]), and molecular dynamics simulations[11,13] indicate that ions do not strongly affect the hydrogen-bond network of water beyond the first solvation shell in salt solutions at high ionic strengths. Bakker and co-workers reported that sulfate dianion,[15] an ion at one extreme end of the Hofmeister series traditionally associated with strong "structure-making" effects, as well as chloride, bromide, and iodide,[16,17] do not significantly affect the reorientation times of water molecules outside the first solvation shell at high ion concentrations. However, more recent results from the same group indicate that cooperative solvation of nearby counterions can lead to longer-ranged patterning of the water network.[18]

The aqueous surface activity of ions has also been linked to Hofmeister effects due to the large difference in dielectric constants at both the liquid−vapor interface and the water−protein interface.[10] Linear spectroscopies are poor probes of the structure of the condensed-phase water surface due to the overwhelmingly stronger signal of the bulk, but sum-frequency generation (SFG) spectroscopy, a second-order optical technique, is more sensitive to and has been used to study the structure of the first few layers of water molecules in pure water[19−23] and ionic solutions.[23−26] Results from SFG spectroscopy,[27] electrospray ionization,[14] and molecular dynamics simulations[28] suggest that some ions, including bromide and iodide,[27,28] are highly surface-active, whereas other ions, notably chloride[27] and sulfate,[26] have lower surface activity, in correlation with the Hofmeister behavior of these ions.

Studying gas-phase hydrated ions offers the advantages that effects of counterions, which can complicate the interpretation of condensed-phase studies, can be eliminated, and intrinsic effects of a single ion or an electron on water can be studied as a function of hydration extent for as many as several hundred attached water molecules.[29,30] Using infrared photodissociation (IRPD) spectroscopy, the structures of many hydrogen-bonded gas-phase ions and complexes, including protonated,[31−38] metal cationized,[31,39−51] and halidated[52] amino acids and peptides, as well as hydrates of small ions,[30,53−78] have been investigated. The hydrogen-stretch region (~2300−4000 cm^{-1}) has proved especially useful, because the frequencies of heteroatom-hydrogen stretching modes are often very sensitive to their hydrogen-bonding environment.

Received: September 15, 2010
Published: March 15, 2011

dx.doi.org/10.1021/ja108341t | J. Am. Chem. Soc. 2011, 133, 4810–4818

Because the proportion of water molecules at the surface of clusters or nanodrops is relatively large, water molecules in which one or both hydrogen atoms do not participate in hydrogen bonds ("free OH" groups), similar to those at the bulk water surface identified in SFG experiments,[7,19−26,79−82] can be studied with IRPD spectroscopy simultaneously with hydrogen-bonded interior water molecules of the same ion−water cluster. IRPD spectroscopy also has the advantage that it provides information similar to linear absorption spectroscopy for such weakly bound systems and can be more directly compared to calculated absorption spectra. Recent results from IRPD spectroscopy indicate that sulfate dianion strongly patterns water molecules beyond the second solvation shell at effective concentrations below 1 M,[75] in contrast to conclusions from condensed-phase femtosecond spectroscopy results obtained at higher concentrations.[15] Other results indicate that, for hydrated ions with water molecules in the second or higher solvation shells, the ion can exhibit properties very similar to those in bulk, such as coordination number,[55,58,65] hydrolysis reactivity,[57,83] and redox properties.[30,84]

Here, we present results from IRPD spectroscopy in the hydrogen stretch region for a total of 17 hydrated anions and cations with charge states between −1 and +3 at fixed cluster size (35−37 attached water molecules), where water molecules are expected to populate the first, second, and third solvation shells. These spectra indicate a strong influence of the ion on the hydrogen-bond network in these nanodrops and a clear dependence of the surface free-OH stretch frequency on ion charge state and size. These results are compared to infrared spectra calculated using two local electric field molecular dynamics models as well as to previously reported gas- and condensed-phase results.

EXPERIMENTAL METHODS

All IRPD spectra were measured using a 2.75 T Fourier-transform ion cyclotron resonance mass spectrometer coupled to a tunable OPO/OPA laser system. The instrument and experimental setup are described in detail elsewhere.[31] Briefly, hydrated ions are generated from 1−5 mM aqueous solutions using nanoelectrospray ionization. Borosilicate capillaries are pulled to an inner tip diameter of ∼1 μm, filled with the solution of interest, and a platinum wire is inserted into the capillary, where it is held in direct contact with the solution at approximately ±600 V relative to the entrance of the instrument. Hydrated ions are guided with electrostatic lenses through five stages of differential pumping into the cell of the mass spectrometer, which is surrounded by a temperature-regulated copper jacket[85] equilibrated to 133 K for at least 8 h prior to each experiment. Ions are trapped and thermalized with the aid of a pulse of dry nitrogen at $\sim 10^{-6}$ Torr, and after a 5−12 s delay, the ion cell returns to a pressure of $<10^{-8}$ Torr.

IRPD spectra were measured using the ensemble average method, which results in spectra directly comparable to those measured for ions of a single cluster size with improved signal-to-noise ratio.[66] Spectra obtained using this method represent average structural features for the range of cluster sizes investigated, reducing the importance of potentially atypical structures associated with "magic number" clusters. Ensembles of hydrated ions containing 35−37 water molecules are isolated using stored waveform inverse Fourier transforms, then irradiated with tunable light between 2950 and 3800 cm^{-1} for 0.85−2.05 s. Background dissociation due to blackbody infrared radiative dissociation (BIRD) and changes in the initial ion ensemble mass spectral distribution are remeasured approximately every 10 min. BIRD rate constants are obtained in the absence of laser radiation as $k_{BIRD} = ((\langle n(t)\rangle - \langle n(0)\rangle)/t)$, where $\langle n(t)\rangle$ is the abundance-weighted average number of water molecules in the ensemble after exposure to the 133 K blackbody field for a time t. Laser-induced photodissociation rate constants are obtained as $k_{las}(\hbar\omega,t_{irr}) = (((\langle n(\hbar\omega,t_{irr})\rangle - \langle n(0)\rangle)/(t_{irr})) - k_{BIRD}$, where t_{irr} is the laser irradiation time, and $\hbar\omega$ is the laser photon energy. All ensemble IRPD spectra are corrected for frequency-dependent variations in laser power.

High-level quantum chemical computations exploring a large conformational space are at present impractical for complexes of this size. Thus, infrared free-OH absorption spectra of $M(H_2O)_{36}$, M = I^-, Cs^+, Co^{2+}, and Mo^{3+}, as well as $Mo^{3+}(H_2O)_{160}$ and $(H_2O)_{1000}$, were modeled using two different methods developed to calculate the spectrum of bulk water.[86,87] After an initial geometry relaxation with molecular mechanics, canonical ensemble molecular dynamics is used to generate 1000 structures at 133 K for each hydrated ion using Impact 5.6 (Schrödinger, LLC, Portland, OR). Each hydrogen/oxygen atom is assigned an electrostatic charge of +0.41/−0.82 e, and the ion is assigned its full formal charge. The projection E_i of the local electric field at a given hydrogen atom H_i due the ion and the hydrogen and oxygen atoms of all other water molecules onto a unit vector in the OH_i bond direction is calculated.

OH stretch spectra are calculated from the cluster geometries and E_i values. In one model,[11,86] the frequency f_i (in cm^{-1}) of the vibrationally uncoupled OH_i stretch is calculated as $f_i = 3745 - 8249 \times E_i$, where E_i is measured in atomic units and the slope and intercept of $f_i(E_i)$ are empirical parameters obtained by fitting bulk Raman spectra. The distribution of absorption frequencies is then obtained as a histogram of f_i values for all 1000 structures. Non-Condon effects (which cause the transition dipole moment to vary with frequency) and both intramolecular and intermolecular vibrational coupling are ignored in this method. In the second model,[87] local OH stretch frequencies are obtained as $f_i = 3762 - 5060 \times E_i - 86\,225 \times E_i^2$, where the coefficients are empirical parameters obtained by fitting frequencies from ab initio computations. Coupling constants for mixing of the two OH stretch local modes in each water molecule are then obtained using these uncoupled mode frequencies as prescribed in ref 87. Relative infrared intensities for the coupled-OH model are calculated as the square magnitude of the transition dipole moment according to ref 87. Although this second spectral model includes intramolecular OH stretch coupling and frequency-dependent absorption intensities, it does not explicitly include intramolecular coupling of the H_2O bend or coupling between different water molecules.

RESULTS AND DISCUSSION

General IRPD OH Stretch Spectral Features. Ensemble IRPD spectra between 2950 and 3800 cm^{-1} measured at 133 K for $M(H_2O)_{35-37}$, M = I^-, tetrabutylammonium (TBA^+), Cs^+, Li^+, Co^{2+}, and La^{3+}, are shown in Figure 1. For nanodrops of this size, the fraction of water molecules located at the surface and, consequently, the surface curvature are very high as compared to bulk water. The relatively high free energy cost associated with such a highly curved surface can potentially cause the hydrogen bonds in the nanodrops to differ from those at the surface and in the interior of bulk water in a number of ways, including typical hydrogen bond strengths, distances, and angles. These differences from bulk neutral water are further affected by the excluded volume, anisotropy, and inhomogeneity of the water network introduced by the ions. We refer to ion-induced structural effects not attributable to excluded volume as ion-induced "patterning". The very broad feature extending from ∼2950−3650 cm^{-1} in each of these spectra is assigned to hydrogen-bonded (HB) OH oscillators, and the sharper features above 3650 cm^{-1} are assigned to free-OH oscillators. For each of these ions, the centroid of the HB band is ∼3420 ± 10 cm^{-1}, and

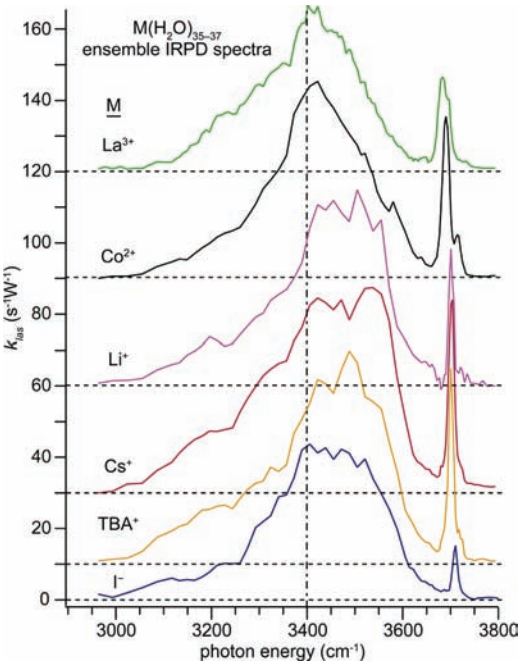

Figure 1. Ensemble IRPD spectra of $M(H_2O)_{35-37}$ at 133 K (TBA^+ = tetrabutylammonium). Infrared absorption maximum for bulk pure water indicated by dash−dot line.

this band has a fwhm of ~250−300 cm^{-1}. The similarity of this feature to the OH stretch infrared spectrum of bulk water (HB band maximum ~3400 cm^{-1})[88] suggests that the water molecules in these hydrated ions form an extensive, largely bulk-like hydrogen-bond network, despite the greater importance of the surface constraint in these clusters versus in bulk solution. The intensity of the HB feature is similar for each of these ions, consistent with experimental and theoretical evidence that water molecule binding energies for clusters of this size are nearly independent of charge state.[89,90]

Ensemble IRPD spectra of the free-OH region (~3640−3760 cm^{-1}) for $M(H_2O)_{35-37}$, M = I^-, Cl^-, HCO_3^-, OH^-, TBA^+, TPA^+, and TMA^+ (=tetrabutyl-, tetrapropyl-, and tetramethylammonium, respectively), Cs^+, Na^+, Li^+, H^+, Ba^{2+}, Ca^{2+}, Co^{2+}, Mg^{2+}, La^{3+}, and Tm^{3+}, are shown in Figure 2. There is no free-OH band for $(SO_4)(H_2O)_n^{2-}$ for n < ~47, indicating that essentially all water molecules in smaller clusters with this ion donate two hydrogen bonds.[75] Dissociation in this region is very weak for the monoanions investigated, consistent with an extensive hydrogen-bond network in which most OH groups are hydrogen-bonded. On the basis of comparison with smaller halide hydrates, the feature at ~3710 cm^{-1} for the anions can be assigned to the free-OH stretch of water molecules that accept two hydrogen bonds and donate a single hydrogen bond (AAD). The AAD band occurs as the dominant free-OH feature at ~3700 cm^{-1} for the monovalent cations, with a shoulder at ~3720 cm^{-1} attributable to water molecules that donate and accept a single hydrogen bond (AD). This AAD feature for the monoanions and monocations is very close to that identified in the SFG spectra of bulk water (~3700−3705 cm^{-1}).[20,23,82] Intense AAD and weaker AD bands are present for the di-/trivalent cations at ~3690/3681 and ~3710/3702 cm^{-1}, respectively, and there are weak acceptor-only water molecule symmetric and antisymmetric stretch bands at ~3646 and 3733 cm^{-1} for the trivalent cations only.

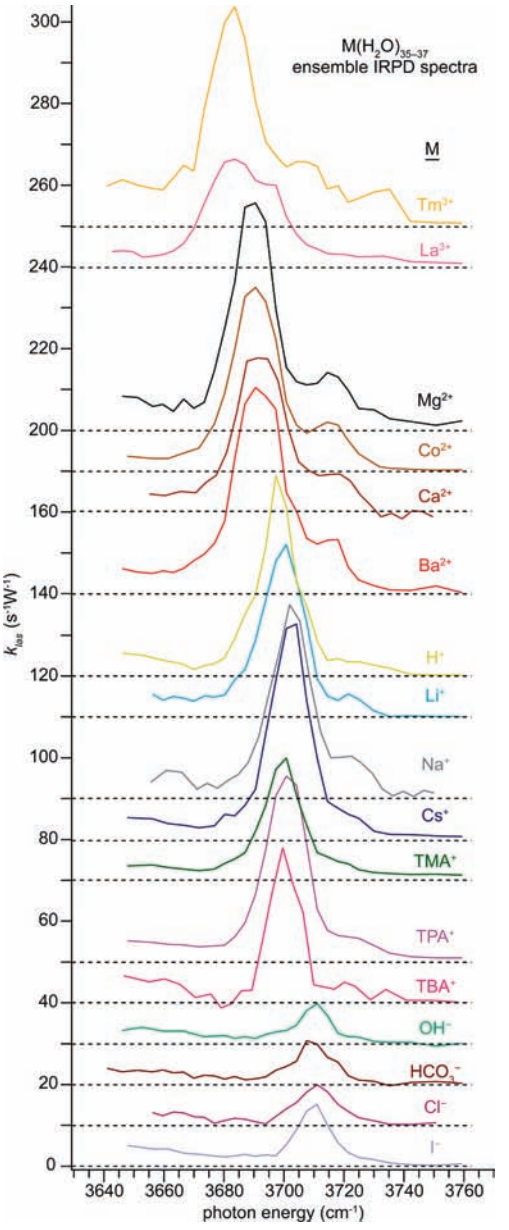

Figure 2. Ensemble IRPD spectra in the free-OH region for $M(H_2O)_{35-37}$ at 133 K (TBA^+, TPA^+, TMA^+ = tetrabutyl-, tetrapropyl-, and tetramethylammonium, respectively).

In aqueous solution[91] as well as in nanodrops generated with electrospray,[14] ions of differing size and polarizability have been reported to have different affinities for the water surface. Because the air−water interface involves a change in dielectric constant similar to that at the protein−water interface, these surface affinity differences have sometimes been associated with Hofmeister series effects.[14] IRPD spectroscopy of small ion hydrates has indicated that some ions, such as TMA^+[67] and Cs^+,[64] tend to favor water−water hydrogen bonding over ion−water interactions, but other ions, such as Li^+[64] and Ca^{2+},[77] are more isotropically solvated. The IRPD spectra of $M(H_2O)_{35-37}$, M = Li^+ and TBA^+ (Figure 1), are quite similar even though the small Li^+ ion might be expected to reside close to the center of the nanodrop and the much larger TBA^+, closer to the surface. Thus, it is difficult to ascertain from these IRPD spectra of nanodrops of

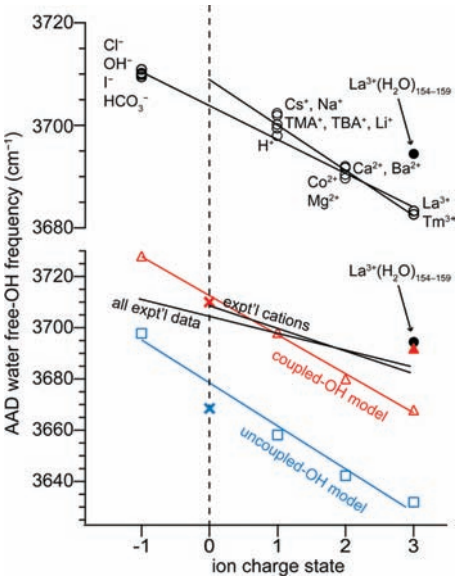

Figure 3. Experimental free-OH stretch frequencies of AAD water molecules for $M(H_2O)_{35-37}$ at 133 K (top; ion labels arranged vertically in correspondence with observed frequencies) and $La^{3+}(H_2O)_{154-159}$ (●). Also shown (bottom) are AAD free-OH frequencies for $M(H_2O)_{36}$ simulations without (□) and with (△) intramolecular OH stretch coupling (see text), as well as for $La^{3+}(H_2O)_{160}$ (▲, coupled-OH model) and $(H_2O)_{1000}$ (plotted for charge state 0; blue/red × indicates coupled/uncoupled-OH model).

this size whether the ions investigated are located at the surface versus the interior.

Stark Shifting of Free-OH Bands for $M(H_2O)_{35-37}$. The AAD free-OH stretch is highest in frequency for the monoanions and red-shifts with increasing charge state for the cations. As shown in Figure 3, where the fitted centroids of the AAD free-OH bands are plotted as a function of ion charge state, the frequency of these bands varies nearly linearly with the charge state of the ion, consistent with Stark shifting of the water AAD free-OH band in quasi-spherical clusters as a result of the ions' Coulomb field. Least-squares fits of the data indicate that the cation AAD free-OH bands follow a more linear relationship with charge than does the entire data set that includes the anions. Similarly, the AAD free-OH frequency for $(SO_4)(H_2O)_{47}^{2-}$, the smallest cluster size at which a free-OH band is observed for this ion,[75] is somewhat less blue-shifted (at ~3710 cm^{-1}) than would be predicted from the trend fitting the cation data. This mild, but significant, difference in AAD free-OH stretch frequencies for anions versus cations suggests that the structures of these nanodrops differ more between anions and cations than among cations of different charge states. This effect may be due to a different orientation of the free-OH groups at the surface of nanodrops with anions as compared to cations. Interestingly, the data for H^+ and OH^- fall near those of the other monatomic ions, despite the potential for H^+ to promote clathrate-like cluster structures[70,78] and for both ions, in principle, to "jump" to different locations in the hydrates via a Grotthuss-type mechanism.[92] Although these nanodrops are cold, they have sufficient initial internal energy to lose a water molecule, which requires more energy than proton transfer between water molecules. The data for TBA^+, TPA^+, and TMA^+ fit the trend of the other cations, even though these hydrophobic ions might be suspected to reside at the "surface" of the water hydrogen-bond network, as with small hydrates of TMA^+.[67] Thus, for all of the hydrated ions investigated, ion charge state is the single most important factor in determining the frequency of the AAD free-OH band at this cluster size.

An extrapolation of these 133 K data to "zero-charge" results in a frequency of 3704.9 cm^{-1} for the AAD free-OH band of a similar-sized neutral water cluster. This value should be close to that for water molecules at the bulk aqueous surface. A fit to the cation data alone clearly overestimates the observed monoanion AAD free-OH band frequencies. Thus, an upper bound of ~3709.7 cm^{-1} for the bulk water AAD free-OH frequency can be estimated from a fit to the cation data. These results are consistent with, although slightly higher than, several reported bulk water free-OH band frequencies from SFG experiments at room temperature.[20,23,82] These values also agree with the AAD free-OH frequency measured for large protonated water clusters[93] as well as for large neutral water clusters generated in supersonic expansions.[94] The Raman[86] and infrared[95] spectra of bulk water are temperature-dependent; thus it may be expected that the 133 K and room temperature free-OH frequency of the bulk water surface may not be identical. However, the free-OH band in SFG is typically much broader than the OH bands measured here, and its frequency and line shape vary with the polarization and angle of incidence of the incoming beams of light due to the dependence of the SFG process on the hyperpolarizability tensor of the surface water molecules.[21] The estimated value (3704.9−3709.7 cm^{-1}) obtained from our IRPD experiments is the first reported experimental frequency of the bulk water free-OH stretch from a thermal, mass-selected cluster population using a linear optical technique akin to absorption spectroscopy.

Effects of Ion Size on Free-OH Ensemble IRPD Spectra. Weak effects of ion size for the monatomic ions are observed. For monatomic ions of a given charge state, a larger ionic radius generally results in a smaller shift from the "zero-charge" free-OH frequency (3704.9 cm^{-1}). This is consistent with the slightly greater distance from the ion at which surface water molecules are located in ion hydrates with a larger ion, resulting in a smaller Stark shift of the OH stretch frequency. For the trivalent cations investigated, ion identity appears to have a much greater effect on the free-OH spectra than for the other ions. In particular, $La^{3+}(H_2O)_{35-37}$ has a substantial shoulder at 3694 cm^{-1} that is not present for $Tm^{3+}(H_2O)_{35-37}$, although the integrated band intensities from 3660 to 3705 cm^{-1} are similar for both ions. The 3694 cm^{-1} band, which appears between the AAD and AD free-OH bands, may be analogous to a similar band appearing in the IRPD spectrum of $Ca^{2+}(H_2O)_{25}$ that decreases in relative intensity or coalesces with the AAD free-OH band for larger hydrates.[58] The absence of such a band for $Tm^{3+}(H_2O)_{35-37}$ suggests a slightly different patterning of surface water molecules by La^{3+} (ionic radius 103.2 pm) versus the slightly smaller Tm^{3+} (88 pm). These two ions have similar IRPD spectra with 20 attached water molecules, despite having different solution-phase coordination numbers (CN = 9 for La^{3+}, 8 for Tm^{3+}) and gas-phase charge-separation reactivity.[57] However, the ensemble IRPD spectra measured here clearly indicate a type of hydrogen-bonding environment for surface water molecules in $La^{3+}(H_2O)_{35-37}$ that is not present to such an extent in $Tm^{3+}(H_2O)_{35-37}$ and may be due to a difference in first solvent shell structure that propagates through the hydrogen-bond network out to the surface water molecules. These ensemble IRPD spectra reflect the structures of at least three adjacent cluster sizes and should have a lesser tendency to represent atypical "magic-number"

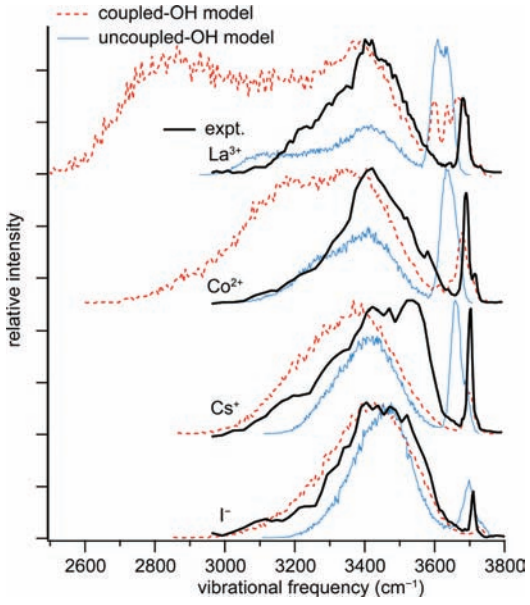

Figure 4. Ensemble IRPD spectra of $M(H_2O)_{35-37}$ and simulated spectra of $M(H_2O)_{36}$ at 133 K, where M is the ion indicated. Thin blue traces represent simulations without vibrational coupling or frequency-dependent transition dipole moments, and dashed red traces represent simulations with intramolecular OH stretch coupling and frequency-dependent transition dipole moments. All spectra are normalized to have the same maximum intensity. Note that Mo^{3+} was used to model La^{3+} because La^{3+} is not implemented in the MD software used for these simulations (see text).

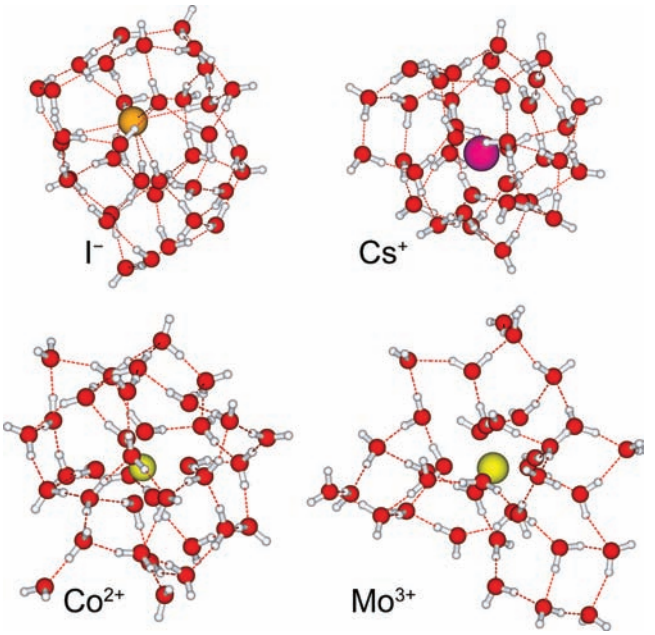

Figure 5. Representative structures for $M(H_2O)_{36}$, M = I^-, Cs^+, Co^{2+}, and Mo^{3+}, from MD simulations used to model ensemble IRPD OH stretch spectra.

cluster structures than IRPD spectra of any one cluster size within this range.[66] Thus, it is possible that $Tm^{3+}(H_2O)_{20}$ and $La^{3+}(H_2O)_{20}$ have similar IRPD spectra and structures although clusters of slightly different size do not.

Modeling Ensemble IRPD Spectra. Simulated infrared spectra for $M(H_2O)_{36}$, M = I^-, Cs^+, Co^{2+}, and Mo^{3+}, are shown in Figure 4, plotted with the corresponding IRPD spectra. Mo^{3+}, which has an ionic radius ~80% of that of Tm^{3+}, was used for the hydrated trivalent metal cation cluster, because lanthanides were not implemented in the software used for the MD simulations at the time they were performed. To our knowledge, this is the first reported application of these electrostatic models, originally parametrized for bonded-OH spectra in condensed-phase systems with periodic boundary conditions,[86,87] to simulate the spectra of isolated hydrated ions in the gas phase. Representative nanodrop structures from the simulations are shown in Figure 5. In the structures generated in the simulations, the ions in these quasi-spherical nanodrops typically have complete or nearly complete first solvation shells with the more highly charged ions closer to the nanodrop center (water network center of mass to ion distance = 48 ± 27, 121 ± 39, 195 ± 143, and 131 ± 67 pm for Mo^{3+}, Co^{2+}, Cs^+, and I^-, respectively).

Qualitatively, the simulated spectra for both the uncoupled and the coupled OH oscillators reproduce the division of the experimental spectra into an intense, broad HB OH stretch region at energies below ~3550 cm^{-1} and a sharp, narrow band close to ~3700 cm^{-1}. Because the uncoupled-OH model does not include frequency-dependent transition dipole moments for individual oscillators, which decrease monotonically with increasing frequency in the coupled-OH model, the uncoupled-OH model generally predicts much greater relative intensity of the free-OH band than does the coupled-OH model. The free-OH bands predicted in the uncoupled-OH model occur at lower frequencies than those in the coupled-OH model, and only the coupled-OH model results in discernible splitting of the free-OH region into subbands (most noticeably for $Mo^{3+}(H_2O)_{36}$).

Investigation of the frequencies calculated for individual water molecules from the clusters used in these coupled-OH simulations reveals that the water hydrogen-bonding states associated with the free-OH region are ordered energetically in the same way as has been determined for many smaller hydrates of gas-phase ions. That is, the symmetric stretch of A-only water molecules is lowest in energy, and the AAD and AD free-OH stretches, as well as A-only antisymmetric stretch, occur at progressively higher energies. Although the total breadth of the calculated free-OH region is considerably larger (by ~70%) for $Mo^{3+}(H_2O)_{36}$ than for the IRPD spectrum of either $La^{3+}(H_2O)_{35-37}$ or $Tm^{3+}(H_2O)_{35-37}$, this model does remarkably well in reproducing this peak series for surface water molecules in gas-phase clusters, given that it is parametrized for bonded-OH stretches in the condensed phase. The free-OH region in these simulations cannot easily be subdivided into hydrogen-bonding states for the uncoupled-OH model, indicating that the experimentally observed splitting arises primarily from intramolecular coupling.

Agreement with the IRPD spectra is especially strong for the $I^-(H_2O)_{36}$ and $Cs^+(H_2O)_{36}$ simulations. Both models resemble the experimental spectra progressively less well with increasing ion charge state (and decreasing ionic radius), predicting a division of the bonded-OH band into two broad subfeatures for the divalent and trivalent cation spectra. The coupled-OH simulations reproduce qualitatively the experimental decrease in the HB OH:free-OH integrated intensity ratio as function of increasing charge state, but the HB OH regions in these simulations are red-shifted from and significantly broader than those observed experimentally for the di- and trivalent cations.

dx.doi.org/10.1021/ja108341t | J. Am. Chem. Soc. 2011, 133, 4810–4818

Comparison of the simulated frequencies of the AAD free-OH bands, plotted with the experimental data in Figure 3, confirms that the electric field of the ion plays a dominant role in the trend in the frequencies with charge state. The uncoupled-OH data are red-shifted considerably from the experimental data, as is the AAD free-OH frequency predicted using this model for a neutral $(H_2O)_{1000}$ cluster (Figure 3, bottom: 3667 cm^{-1}), which is greatly red-shifted from the range of AAD free-OH frequencies measured for hydrated gas-phase ions using IRPD spectroscopy and the bulk water and ice surfaces using SFG spectroscopy. This band occurs at 3710 cm^{-1} for the coupled-OH model (Figure 3, bottom), in excellent agreement with both the extrapolated zero-charge value from these experimental data (vide supra) and SFG experiments.[20,23,82] The coupled-OH model predicts a slope in the AAD frequency as a function of ion charge state (−15.3 cm^{-1} per elementary charge) similar to that of the uncoupled-OH model (−13.1). Both of these are larger in magnitude than the experimental value (−9.3 for the cation data), although the coupled-OH model is much closer in absolute frequency to the experimental data. This model predicts a frequency of 3692 cm^{-1} for the AAD free-OH band of La^{3+}-$(H_2O)_{154-159}$, in excellent agreement with the experimental value of 3694.9 cm^{-1} (Figure 3, bottom), and a gentler slope (−6 cm^{-1} per elementary charge) is predicted for clusters of this size, consistent with a weaker effect of the ion's electric field on surface water molecules as the droplet radius increases.

These results indicate that, as for the condensed phase,[11,13,86,87] the local electric field experienced by the hydrogen atoms in these clusters largely accounts for the stretching frequencies of their associated OH groups, and that intramolecular coupling[87] likely plays a large role in the splitting observed for the free-OH region. This is consistent with the Stark-shifting of surface water molecule free-OH frequencies observed in the IRPD data. Despite the limitations inherent in a point charge model using structures obtained by molecular dynamics, neither of which includes polarizability, the resulting effect of the electric field at each H atom on the OH stretch frequency appears to account for the effect of ion charge and screening by water, at least for the singly charged ions. However, although these models qualitatively reproduce some of the features of the experimental hydrated ion spectra, they do not resemble experiment closely enough for detailed spectral analysis. In particular, it should be emphasized that the use of the full ion charge state for multivalent monatomic ions is likely inappropriate in these models for ions with ∼3−4 hydration shells due to polarization of first-shell solvent molecules and/or charge transfer effects, which reduce the electric field contribution of these ions to the Stark shift of surrounding water molecules. Polarization of the ions themselves likely occurs to some extent, especially for Cs^+ and I^-, which may affect the structure and spectra of the experimental nanodrops but is not included in these models. These discrepancies are likely mitigated for larger clusters, where a greater fraction of the water molecules are located far from the central ion and first solvation shell. Furthermore, because the initial internal energy of the clusters investigated is much higher than the barrier for loss of a water molecule, the IRPD intensities in the experimental spectra should resemble linear absorption spectra, although the correspondence may not be exact for a variety of reasons. Thus, the poor match in relative intensities of the HB and free-OH regions in comparison to experiment for either model suggests that a more sophisticated model of the frequency-dependence of transition dipole moments[87] is necessary to accurately model these relative intensities.

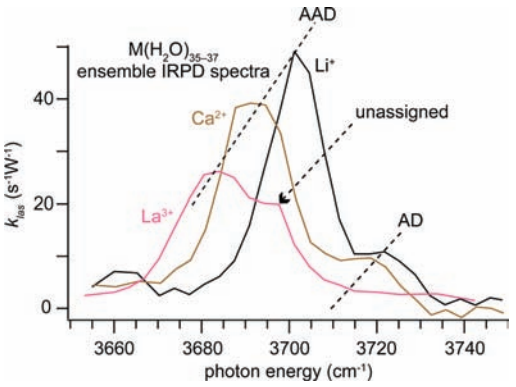

Figure 6. Ensemble IRPD spectra in the free-OH region for $M(H_2O)_{35-37}$, M = Li^+ (black), Ca^{2+} (brown), and La^{3+} (magenta). Dashed lines connecting the maxima of free-OH bands corresponding to different hydrogen-bonding motifs illustrate the effect of ion charge state on band frequencies (i.e., the Stark shift).

Scheme 1. Ion-Induced Patterning Motifs for Water Molecules in the First Solvation Shell of Gas-Phase Sulfate, Calcium, and Tetramethylammonium Ions

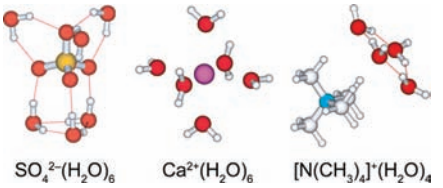

Excluded Volume Effects and Ion-Induced Patterning of the Cluster Surface. IRPD spectra in the free-OH region for $M(H_2O)_{35-37}$, M = Na^+, Ca^{2+}, and La^{3+}, are shown in Figure 6. These ions have nearly identical ionic radii (102, 100, and 103 pm, respectively), although they do have slightly different coordination numbers (∼6−9).[58,96,97] Because these ions are essentially the same size, the excluded volume in the nanodrops introduced by these ions should be nearly identical. Thus, any differences in the structures of these nanodrops should not be the result of excluded volume effects but rather ion-induced patterning of the water network. Such patterning, represented in Scheme 1 for ions with different charge states, has been reported for many small hydrated ions with partial first and second solvation shells.[55,64,65,75−77,98,99] All three ions have strong AAD free-OH bands, which are Stark-shifted by different amounts due to the different charge states of these three ions. The spectra for Na^+ and Ca^{2+} also have strong, Stark-shifted AD free-OH bands, although no strong band is observed for La^{3+} despite the presence of a strong band for Tm^{3+} (ionic radius 88 pm) at 3702 cm^{-1} (vide supra). The spectrum for La^{3+} has a band at 3694 cm^{-1} between the AAD band and the expected AD free-OH frequency (∼3702 cm^{-1}). Because charge state plays a larger role in the frequencies of free-OH bands for different hydrogen-bonding motifs in these nanodrops than does ion size (vide supra), this 3694 cm^{-1} band cannot represent the same type of AD free-OH group observed for Na^+, Ca^{2+}, and Tm^{3+}. Although it is difficult to assign this band to surface water molecules with a specific hydrogen-bonding environment, both the presence of this unique band and the lack of a distinct AD band for

dx.doi.org/10.1021/ja108341t | J. Am. Chem. Soc. 2011, 133, 4810–4818

La^{3+} indicate that a significant number of water molecules at the surface of the La^{3+}-containing nanodrops exist in a hydrogen-bonding environment not observed for Na^+ or Ca^{2+}. These results indicate that La^{3+} affects distant surface water molecules several solvation shells away from the ion in a manner that is not attributable solely to the surface constraint of the nanodrops or excluded volume of the ion.

Further Evidence for Ion-Induced Patterning of the Nanodrop Surface. The IRPD spectra of the other ions investigated as well as the modeled structures provide additional evidence that ion-induced patterning occurs in nanodrops of this size for many ions. Perhaps most dramatic is the much lower intensity of the free-OH band (~3710 cm^{-1}) for $I^-(H_2O)_{35-37}$ than for the positively charged clusters. The integrated free-OH band intensity for I^- makes up about 2% of the total integrated intensity of the entire OH stretch spectrum, whereas it is much larger (~6−10%) for the monatomic cations investigated. Because free-OH band intensities in the IRPD spectra are a function of both the number of free-OH oscillators with a given frequency as well as electric field effects on transition dipole moments, these differences in integrated free-OH intensities cannot be attributed to either of these factors exclusively, but the modeled structures indicate that there are significantly fewer free-OH groups at the nanodrop surface for anions. The modeled structures indicate that ~9% of the OH groups in the nanodrops with I^- are free-OH groups, whereas this number is ~22%, 30%, and 40% for Cs^+, Co^{2+}, and Mo^{3+}, respectively. Although the differences in these values from the simulation may be exaggerated due to the lack of ion and water molecule polarizability in the model, this trend suggests that the low relative intensity for the experimental free-OH band of $I^-(H_2O)_{35-37}$ can be predominantly attributed to a significantly smaller number of surface free-OH groups than for the cations investigated.

The increase in the number of free-OH groups at the surface of the modeled nanodrops with increasing ion charge state is consistent with stronger patterning of water for more highly charged ions. Divalent metal cations with partial first and second solvation shells tend to adopt structures with relatively few water−water hydrogen bonds,[55,65,77,100] but Cs^{+64} and other large monocations, such as ammonium[78,101] and tetramethylammonium (TMA^+),[67] have been shown to have a much weaker patterning effect, favoring water−water hydrogen bonding over water−ion interactions even for small clusters. Hydrogen bonding between first solvation shell water molecules is also very common for small halide hydrate clusters.[53,59,69]

Further evidence for ion-induced water patterning is apparent within the hydrogen-bonded feature in these spectra. The ensemble IRPD spectra of $M(H_2O)_{35-37}$, M = I^-, TBA^+, Cs^+, and Li^+, each have significantly greater relative intensity between 3500 and 3600 cm^{-1} than do the spectra for M = Co^{2+} and La^{3+} (Figure 1). Recent computational models of infrared[87] and Raman[86] spectra of bulk water indicate that this spectral region is associated with water molecules that are less strongly hydrogen bonded than OH oscillators at lower frequencies. The more highly charged Co^{2+} and La^{3+} ions induce a greater polarization of inner-shell water molecules, so it is likely that these ions also strengthen hydrogen bonds at a greater distance from the ion than do M = I^-, TBA^+, Cs^+, and Li^+, shifting intensity from the 3500−3600 cm^{-1} region to lower energy. (Intensity in this region has also been attributed to the HB OH stretch of AD water molecules in five-member rings, as reported for small, protonated water clusters[102] and $Ni^+(H_2O)_n$, $11 \le n \le 21$.[71]) Ion-induced patterning of the water hydrogen-bond network beyond the second solvation shell has recently been reported on the basis of ensemble IRPD spectra of $(SO_4^{2-})(H_2O)_n$,[75] and these results suggest that such patterning is intrinsic to many ions of various charge states, where it may be in part responsible for bulk ionic solution properties such as Hofmeister effects.

CONCLUSIONS

IRPD ensemble spectra in the OH stretch region for $M(H_2O)_{35-37}$, M = I^-, Cl^-, HCO_3^-, OH^-, tetrabutyl-, tetrapropyl-, and tetramethylammonium, Cs^+, Na^+, Li^+, H^+, Ba^{2+}, Ca^{2+}, Co^{2+}, Mg^{2+}, La^{3+}, and Tm^{3+}, measured at an ion cell temperature of 133 K reveal that these clusters all have extensive bulk-like hydrogen-bond networks with surface structures that depend on the charge-state, and, to a lesser extent, the size, of the ion. Water molecules accepting two and donating hydrogen bond (AAD) are significantly more abundant at the surface of these ions than are AD water molecules, and evidence of A-only water molecules is observed only for the trivalent metal cations. The frequency of the AAD free-OH feature shifts nearly linearly with ion charge state, consistent with a Stark shift induced by the electrostatic field of the ion. The similarity of the hydrogen-bonded OH feature in these spectra to the infrared spectrum of liquid water as opposed to ice I[95] suggests that the water network in clusters of this size is liquid-like or is poorly described by either condensed-phase structure, because the ion and inner solvation shell(s) prevent the development of an extensive pseudocrystalline water network for hydrates of this size. This result is consistent with a melting point depression, such as that for $(H_2O)_n^-$, n = 48 and 118, for which melting point transitions at 93 and 118 K, respectively, were recently reported,[103] and with water binding energies for hydrated divalent metal cations that are closer to the bulk heat of vaporization of water than of ice for n > ~40.[89] Because these clusters are formed by solvent evaporation from electrospray droplets initially at room temperature, rapid evaporative cooling may kinetically trap these clusters into structures that are more like bulk liquid than ice. Ion-induced patterning of the water molecule network that is not attributable to excluded volume effects propagates from the first solvation shell to the surface of these clusters and is more dramatic for ions of higher charge state, as reported previously for large hydrated sulfate dianion clusters,[75] and is consistent with reported halide ion-induced patterning in bulk ionic solutions that is not reflected strongly in OH-stretch Raman spectra.[11] These results contrast with reports based on femtosecond OH vibrational anisotropy decay experiments that ion-induced patterning of the bulk water network is "negligible" beyond the first solvation shell[15,16] and indicate that cooperative solvation of nearby strongly hydrated, multivalent counterions[18] is not a necessary condition for such patterning in solution.

These results also serve as a stringent benchmark for theoretical modeling of hydrated ion and bulk solution properties. Spectra for these ions modeled using two combined MD and electrostatic approaches originally designed for bulk solutions reproduce the division of the spectrum into a broad bonded-OH feature and a narrow free-OH feature, both of which red-shift with increasing charge state of the ion. In particular, Stark-shifting of surface water molecule free-OH bands is predicted by both models, and splitting of the free-OH region into bands associated with different hydrogen-bonding motifs is qualitatively reproduced in the coupled-OH model. Neither set of modeled spectra resembles the IRPD

spectra consistently for all ions, although agreement is better for the monoanions and monocations than for the di- or trivalent cations. These results suggest that electrostatic models that include vibrational coupling and that further account for polarizing and/or charge transfer effects of highly charged ions in clusters of this size must be used to accurately model IRPD spectra. Such models could obviate the need for computationally expensive ab initio calculations and facilitate interpretation of hydrated ion IRPD spectra as well as improve the accuracy of modeling the effects of ions in solution.

AUTHOR INFORMATION

Corresponding Author
williams@cchem.berkeley.edu

ACKNOWLEDGMENT

We thank Prof. Phillip L. Geissler for helpful discussions and the National Science Foundation (grants CHE-1012833 and CHE-0840505) for generous financial support.

REFERENCES

(1) Kunz, W.; Henle, J.; Ninham, B. W. *Curr. Opin. Colloid Interface Sci.* **2004**, *9*, 19–37.
(2) Collins, K. D. *Biophys. J.* **1997**, *72*, 65–76.
(3) Schott, H. *J. Colloid Interface Sci.* **1973**, *43*, 150–155.
(4) Grigorjev, P. A.; Bezrukov, S. M. *Biophys. J.* **1994**, *67*, 2265–2271.
(5) Baldwin, R. L. *Biophys. J.* **1996**, *71*, 2056–2063.
(6) Cacace, M. G.; Landau, E. M.; Ramsden, J. J. *Q. Rev. Biophys.* **1997**, *30*, 241–277.
(7) Chen, X.; Yang, T.; Kataoka, S.; Cremer, P. S. *J. Am. Chem. Soc.* **2007**, *129*, 12272–12279.
(8) Collins, K. D. *Methods* **2004**, *34*, 300–311.
(9) Freire, M. G.; Neves, C. M. S. S.; Silva, A. M. S.; Santos, L. M. N. B. F.; Marrucho, I. M.; Rebelo, L. P. N.; Shah, J. K.; Maginn, E. J.; Coutinho, J. A. P. *J. Phys. Chem. B* **2010**, *114*, 2004–2014.
(10) Pegram, L. M.; Record, M. T. *J. Phys. Chem. B* **2007**, *111*, 5411–5417.
(11) Smith, J. D.; Saykally, R. J.; Geissler, P. L. *J. Am. Chem. Soc.* **2007**, *129*, 13847–13856.
(12) Uejio, J. S.; Schwartz, C. P.; Duffin, A. M.; Drisdell, W. S.; Cohen, R. C.; Saykally, R. J. *Proc. Natl. Acad. Sci. U.S.A.* **2008**, *105*, 6809–6812.
(13) Lin, Y. S.; Auer, B. M.; Skinner, J. L. *J. Chem. Phys.* **2009**, *131*, 144511.
(14) Cheng, J.; Vecitis, C. D.; Hoffmann, M. R.; Colussi, A. J. *J. Phys. Chem. B* **2006**, *110*, 25598–25602.
(15) Omta, A. W.; Kropman, M. F.; Woutersen, S.; Bakker, H. J. *Science* **2003**, *301*, 347–349.
(16) Omta, A. W.; Kropman, M. F.; Woutersen, S.; Bakker, H. J. *J. Chem. Phys.* **2003**, *119*, 12457–12461.
(17) Bakker, H. J.; Kropman, M. F.; Omta, A. W. *J. Phys.: Condens. Matter* **2005**, *17*, S3215–S3224.
(18) Tielrooij, K. J.; Garcia-Araez, N.; Bonn, M.; Bakker, H. J. *Science* **2010**, *328*, 1006–1009.
(19) Ji, N.; Ostroverkhov, V.; Chen, C. Y.; Shen, Y. R. *J. Am. Chem. Soc.* **2007**, *129*, 10056–10057.
(20) Ji, N.; Ostroverkhov, V.; Tian, C. S.; Shen, Y. R. *Phys. Rev. Lett.* **2008**, *100*, 096102.
(21) Wei, X.; Miranda, P. B.; Shen, Y. R. *Phys. Rev. Lett.* **2001**, *86*, 1554–1557.
(22) Tian, C. S.; Shen, Y. R. *J. Am. Chem. Soc.* **2009**, *131*, 2790–2791.
(23) Gopalakrishnan, S.; Liu, D. F.; Allen, H. C.; Kuo, M.; Shultz, M. J. *Chem. Rev.* **2006**, *106*, 1155–1175.
(24) Schnitzer, C.; Baldelli, S.; Shultz, M. J. *J. Phys. Chem. B* **2000**, *104*, 585–590.
(25) Shultz, M. J.; Schnitzer, C.; Simonelli, D.; Baldelli, S. *Int. Rev. Phys. Chem.* **2000**, *19*, 123–153.
(26) Gopalakrishnan, S.; Jungwirth, P.; Tobias, D. J.; Allen, H. C. *J. Phys. Chem. B* **2005**, *109*, 8861–8872.
(27) Liu, D. F.; Ma, G.; Levering, L. M.; Allen, H. C. *J. Phys. Chem. B* **2004**, *108*, 2252–2260.
(28) Jungwirth, P. *Faraday Discuss.* **2009**, *141*, 9–30.
(29) Griffin, G. B.; Young, R. M.; Ehrler, O. T.; Neumark, D. M. *J. Chem. Phys.* **2009**, *131*, 194302.
(30) Donald, W. A.; Leib, R. D.; Demireva, M.; O'Brien, J. T.; Prell, J. S.; Williams, E. R. *J. Am. Chem. Soc.* **2009**, *131*, 13328–13337.
(31) Bush, M. F.; O'Brien, J. T.; Prell, J. S.; Saykally, R. J.; Williams, E. R. *J. Am. Chem. Soc.* **2007**, *129*, 1612–1622.
(32) Fujihara, A.; Matsumoto, H.; Shibata, Y.; Ishikawa, H.; Fuke, K. *J. Phys. Chem. A* **2008**, *112*, 1457–1463.
(33) Lucas, B.; Grégoire, G.; Lemaire, J.; Maitre, P.; Glotin, F.; Schermann, J. P.; Desfrançois, C. *Int. J. Mass Spectrom.* **2005**, *243*, 105–113.
(34) Prell, J. S.; O'Brien, J. T.; Steill, J. D.; Oomens, J.; Williams, E. R. *J. Am. Chem. Soc.* **2009**, *131*, 11442–11449.
(35) Vaden, T. D.; de Boer, T. S. J. A.; Simons, J. P.; Snoek, L. C.; Suhai, S.; Paizs, B. *J. Phys. Chem. A* **2008**, *112*, 4608–4616.
(36) Dunbar, R. C.; Steill, J. D.; Polfer, N. C.; Oomens, J. *Int. J. Mass Spectrom.* **2009**, *283*, 77–84.
(37) Prell, J. S.; Chang, T. M.; O'Brien, J. T.; Williams, E. R. *J. Am. Chem. Soc.* **2010**, *132*, 7811–7819.
(38) Stearns, J. A.; Boyarkin, O. V.; Rizzo, T. R. *J. Am. Chem. Soc.* **2007**, *129*, 13820–13821.
(39) Armentrout, P. B.; Rodgers, M. T.; Oomens, J.; Steill, J. D. *J. Phys. Chem. A* **2008**, *112*, 2248–2257.
(40) Balaj, O. P.; Kapota, C.; Lemaire, J.; Ohanessian, G. *Int. J. Mass Spectrom.* **2008**, *269*, 196–209.
(41) Bush, M. F.; Prell, J. S.; Saykally, R. J.; Williams, E. R. *J. Am. Chem. Soc.* **2007**, *129*, 13544–13553.
(42) Carl, D. R.; Cooper, T. E.; Oomens, J.; Steill, J. D.; Armentrout, P. B. *Phys. Chem. Chem. Phys.* **2010**, *12*, 3384–3398.
(43) Drayss, M. K.; Blunk, D.; Oomens, J.; Schäfer, M. *J. Phys. Chem. A* **2008**, *112*, 11972–11974.
(44) Dunbar, R. C.; Steill, J. D.; Polfer, N. C.; Oomens, J. *J. Phys. Chem. B* **2009**, *113*, 10552–10554.
(45) Forbes, M. W.; Bush, M. F.; Polfer, N. C.; Oomens, J.; Dunbar, R. C.; Williams, E. R.; Jockusch, R. A. *J. Phys. Chem. A* **2007**, *111*, 11759–11770.
(46) Kapota, C.; Lemaire, J.; Maitre, P.; Ohanessian, G. *J. Am. Chem. Soc.* **2004**, *126*, 1836–1842.
(47) Nicely, A. L.; Miller, D. J.; Lisy, J. M. *J. Am. Chem. Soc.* **2009**, *131*, 6314–6315.
(48) O'Brien, J. T.; Prell, J. S.; Steill, J. D.; Oomens, J.; Williams, E. R. *J. Phys. Chem. A* **2008**, *112*, 10823–10830.
(49) Polfer, N. C.; Paizs, B.; Snoek, L. C.; Compagnon, I.; Suhai, S.; Meijer, G.; von Helden, G.; Oomens, J. *J. Am. Chem. Soc.* **2005**, *127*, 8571–8579.
(50) Prell, J. S.; Demireva, M.; Williams, E. R. *J. Am. Chem. Soc.* **2009**, *131*, 1232–1242.
(51) Prell, J. S.; Flick, T. G.; Oomens, J.; Berden, G.; Williams, E. R. *J. Phys. Chem. A* **2010**, *114*, 854–860.
(52) O'Brien, J. T.; Prell, J. S.; Berden, G.; Oomens, J.; Williams, E. R. *Int. J. Mass Spectrom.* **2010**, *297*, 116–123.
(53) Ayotte, P.; Bailey, C. G.; Weddle, G. H.; Johnson, M. A. *J. Phys. Chem. A* **1998**, *102*, 3067–3071.
(54) Ayotte, P.; Weddle, G. H.; Bailey, C. G.; Johnson, M. A.; Vila, F.; Jordan, K. D. *J. Chem. Phys.* **1999**, *110*, 6268–6277.
(55) Bush, M. F.; O'Brien, J. T.; Prell, J. S.; Wu, C. C.; Saykally, R. J.; Williams, E. R. *J. Am. Chem. Soc.* **2009**, *131*, 13270–13277.
(56) Bush, M. F.; Oomens, J.; Saykally, R. J.; Williams, E. R. *J. Am. Chem. Soc.* **2008**, *130*, 6463–6471.
(57) Bush, M. F.; Saykally, R. J.; Williams, E. R. *J. Am. Chem. Soc.* **2008**, *130*, 9122–9128.

(58) Bush, M. F.; Saykally, R. J.; Williams, E. R. *J. Am. Chem. Soc.* **2008**, *130*, 15482–15489.
(59) Cabarcos, O. M.; Weinheimer, C. J.; Lisy, J. M.; Xantheas, S. S. *J. Chem. Phys.* **1999**, *110*, 5–8.
(60) Choi, J. H.; Kuwata, K. T.; Cao, Y. B.; Okumura, M. *J. Phys. Chem. A* **1998**, *102*, 503–507.
(61) Elliott, B. M.; Relph, R. A.; Roscioli, J. R.; Bopp, J. C.; Gardenier, G. H.; Guasco, T. L.; Johnson, M. A. *J. Chem. Phys.* **2008**, *129*, 094303.
(62) Headrick, J. M.; Diken, E. G.; Walters, R. S.; Hammer, N. I.; Christie, R. A.; Cui, J.; Myshakin, E. M.; Duncan, M. A.; Johnson, M. A.; Jordan, K. D. *Science* **2005**, *308*, 1765–1769.
(63) Iino, T.; Ohashi, K.; Inoue, K.; Judai, K.; Nishi, N.; Sekiya, H. *J. Chem. Phys.* **2007**, *126*, 194302.
(64) Miller, D. J.; Lisy, J. M. *J. Am. Chem. Soc.* **2008**, *130*, 15393–15404.
(65) O'Brien, J. T.; Williams, E. R. *J. Phys. Chem. A* **2008**, *112*, 5893–5901.
(66) Prell, J. S.; O'Brien, J. T.; Williams, E. R. *J. Am. Soc. Mass Spectrom.* **2010**, *21*, 800–809.
(67) Prell, J. S.; Williams, E. R. *J. Am. Chem. Soc.* **2009**, *131*, 4110–4119.
(68) Robertson, W. H.; Diken, E. G.; Price, E. A.; Shin, J. W.; Johnson, M. A. *Science* **2003**, *299*, 1367–1372.
(69) Robertson, W. H.; Johnson, M. A. *Annu. Rev. Phys. Chem.* **2003**, *54*, 173–213.
(70) Shin, J. W.; Hammer, N. I.; Diken, E. G.; Johnson, M. A.; Walters, R. S.; Jaeger, T. D.; Duncan, M. A.; Christie, R. A.; Jordan, K. D. *Science* **2004**, *304*, 1137–1140.
(71) Walters, R. S.; Pillai, E. D.; Duncan, M. A. *J. Am. Chem. Soc.* **2005**, *127*, 16599–16610.
(72) Wang, Y. S.; Chang, H. C.; Jiang, J. C.; Lin, S. H.; Lee, Y. T.; Chang, H. C. *J. Am. Chem. Soc.* **1998**, *120*, 8777–8788.
(73) Wang, Y. S.; Tsai, C. H.; Lee, Y. T.; Chang, H. C.; Jiang, J. C.; Asvany, O.; Schlemmer, S.; Gerlich, D. *J. Phys. Chem. A* **2003**, *107*, 4217–4225.
(74) Wu, C. C.; Lin, C. K.; Chang, H. C.; Jiang, J. C.; Kuo, J. L.; Klein, M. L. *J. Chem. Phys.* **2005**, *122*, 074315.
(75) O'Brien, J. T.; Prell, J. S.; Bush, M. F.; Williams, E. R. *J. Am. Chem. Soc.* **2010**, *132*, 8248–8249.
(76) Bush, M. F.; Saykally, R. J.; Williams, E. R. *J. Am. Chem. Soc.* **2007**, *129*, 2220–2221.
(77) Bush, M. F.; Saykally, R. J.; Williams, E. R. *ChemPhysChem* **2007**, *8*, 2245–2253.
(78) Diken, E. G.; Hammer, N. I.; Johnson, M. A.; Christie, R. A.; Jordan, K. D. *J. Chem. Phys.* **2005**, *123*, 164309.
(79) Noah-Vanhoucke, J.; Smith, J. D.; Geissler, P. L. *J. Phys. Chem. B* **2009**, *113*, 4065–4074.
(80) Morita, A.; Hynes, J. T. *Chem. Phys.* **2000**, *258*, 371–390.
(81) Morita, A.; Hynes, J. T. *J. Phys. Chem. B* **2002**, *106*, 673–685.
(82) Raymond, E. A.; Richmond, G. L. *J. Phys. Chem. B* **2004**, *108*, 5051–5059.
(83) Donald, W. A.; Leib, R. D.; O'Brien, J. T.; Williams, E. R. *Chem.-Eur. J.* **2009**, *15*, 5926–5934.
(84) Donald, W. A.; Leib, R. D.; O'Brien, J. T.; Bush, M. F.; Williams, E. R. *J. Am. Chem. Soc.* **2008**, *130*, 3371–3381.
(85) Wong, R. L.; Paech, K.; Williams, E. R. *Int. J. Mass Spectrom.* **2004**, *232*, 59–66.
(86) Smith, J. D.; Cappa, C. D.; Wilson, K. R.; Cohen, R. C.; Geissler, P. L.; Saykally, R. J. *Proc. Natl. Acad. Sci. U.S.A.* **2005**, *102*, 14171–14174.
(87) Yang, M.; Skinner, J. L. *Phys. Chem. Chem. Phys.* **2010**, *12*, 982–991.
(88) Freda, M.; Piluso, A.; Santucci, A.; Sassi, P. *Appl. Spectrosc.* **2005**, *59*, 1155–1159.
(89) Donald, W. A.; Leib, R. D.; Demireva, M.; Negru, B.; Neumark, D. M.; Williams, E. R. *J. Phys. Chem. A* **2011**, *115*, 2–12.
(90) Donald, W. A.; Williams, E. R. *J. Phys. Chem. A* **2008**, *112*, 3515–3522.
(91) Jungwirth, P.; Winter, B. *Annu. Rev. Phys. Chem.* **2008**, *59*, 343–366.
(92) Marx, D. *ChemPhysChem* **2006**, *7*, 1848–1870.
(93) Mizuse, K.; Fujii, A.; Mikami, N. *J. Chem. Phys.* **2007**, *126*, 231101.
(94) Buch, V.; Bauerecker, S.; Devlin, J. P.; Buck, U.; Kazimirski, J. K. *Int. Rev. Phys. Chem.* **2004**, *23*, 375–433.
(95) Brubach, J. B.; Mermet, A.; Filabozzi, A.; Gerschel, A.; Roy, P. *J. Chem. Phys.* **2005**, *122*, 184509.
(96) Spedding, F. H.; Pikal, M. J.; Ayers, B. O. *J. Phys. Chem.* **1966**, *70*, 2440–2449.
(97) Mhin, B. J.; Kim, J.; Kim, K. S. *Chem. Phys. Lett.* **1993**, *216*, 305–308.
(98) Miller, D. J.; Lisy, J. M. *J. Chem. Phys.* **2006**, *124*, 024319.
(99) Miller, D. J.; Lisy, J. M. *J. Am. Chem. Soc.* **2008**, *130*, 15381–15392.
(100) Cooper, T. E.; Carl, D. R.; Armentrout, P. B. *J. Phys. Chem. A* **2009**, *113*, 13727–13741.
(101) Chang, H. C.; Wang, Y. S.; Lee, Y. T.; Chang, H. C. *Int. J. Mass Spectrom.* **1998**, *180*, 91–102.
(102) Jiang, J. C.; Wang, Y. S.; Chang, H. C.; Lin, S. H.; Lee, Y. T.; Niedner-Schatteburg, G.; Chang, H. C. *J. Am. Chem. Soc.* **2000**, *122*, 1398–1410.
(103) Hock, C.; Schmidt, M.; Kuhnen, R.; Bartels, C.; Ma, L.; Haberland, H.; von Issendorff, B. *Phys. Rev. Lett.* **2009**, *103*, 073401.